Supporting information

Characterization:

The morphology and structure of these obtained samples were characterized using X-ray diffraction (Rigaku D/Max-2500) and transmission electron microscopy (Thermo Talos F200X) equipped with energy dispersive spectroscopy. The specific surface area and pore size distribution were analyzed using the Brunauer–Emmett–Teller (BET NOVA2200e) method, where the specific surface area was calculated using the multipoint BET method and the pore size distribution was determined using non-local density functional theory (NLDFT). The degree of graphitization of the samples was assessed using Senterra Raman spectroscopy. The elemental composition and oxidation states of the samples were analyzed using X-ray photoelectron spectroscopy (XPS, Thermo Fisher Scientific Nexsa G2).

Rh K-edge X-ray absorption fine structure (XAFS) analyses were conducted with Si(111) crystal monochromators at the BL14W beamline at the Shanghai Synchrotron Radiation Facility (SSRF) in Shanghai, China. Prior to XAFS analysis, samples were placed in aluminum holders and sealed with Kapton tape. The XAFS spectra were recorded at room temperature using a 4-channel Silicon Drift Detector (SDD, Bruker 5040) in transmission/fluorescence mode. Minimal changes in the line shape and peak position of the Rh K-edge XANES spectra were observed between two scans of a specific sample. The XAFS spectra of standard samples were recorded in transmission mode and subsequently processed and analyzed using dedicated software.

Thermogravimetric analysis (TGA) was conducted using the SDT Q600 from TA Instruments (USA). Approximately 3 mg of sample was placed in a crucible and subjected to heating under a nitrogen atmosphere at a flow rate of 100 mL/min. NC-Rh1 sample was obtained by heating at a rate of 5°C/min up to 275°C and held for 5 hours, while Rh-N-C was obtained at a rate of 2°C/min up to 550°C and held for 5 hours.

Electrochemical Testing:

Electrochemical tests were conducted using a CHI 760e electrochemical workstation in

a three-electrode system, with 0.1 M $HClO_4$ as the electrolyte at room temperature of 25°C. A rotating disk electrode (RDE, d=5 mm), platinum wire, and a pre-calibrated saturated calomel electrode were employed as the working, counter and reference electrodes, respectively. A mixture of 2 mg catalyst together with x mg XC-72(where x = 0.2, 0.6, 1.0, 1.4, 1.8, 2.2, 2.6, 3.0, 3.4), 1 ml of anhydrous ethanol, and 10 μl of 5% Nafion® was sonicated for over 30 minutes to form a homogeneous slurry. A 25 μl aliquot of the slurry was deposited onto the glassy carbon surface of the RDE, and then drying in air naturally to evaporate the solvent. Linear sweep voltammetry (LSV) tests were conducted in N_2 or CO-saturated 0.1 M $HClO_4$ solution with a potential window of 0-0.7 V (vs. RHE) at a scan rate of 10 mV/s. Cyclic voltammetry (CV) tests were performed in N_2-saturated 0.1 M $HClO_4$ solution with a potential window of 0-0.3 V (vs. RHE) at a scan rate of 100 mV/s.

The catalyst was tested in a high-temperature proton exchange membrane fuel cell (HT-PEMFC), with Rh-N-C (0.84 wt% and 2.88 wt%) serving as the anode catalyst, with metal loadings of 20 μg/cm^2 and 60 μg/cm^2, respectively, or commercial Pt/C catalyst with a metal loading of 0.7 mg/cm^2. The Rh-N-C was mixed with equal mass of XC-72 carbon powder and polytetrafluoroethylene (PTFE), which was added as a binder, with an ethanol-water mixed solution serving as the solvent. After thorough sonication, the mixture was uniformly sprayed onto the gas diffusion layer (GDL) as the anode, while PtCo/C was used as the cathode catalyst with a Pt loading of 1.5 mg/cm^2. The membrane electrode assembly (MEA) was constructed using the anode, a H_3PO_4 doped AP40 membrane, and the cathode, followed by hot pressing at 130°C for 5 minutes. During testing, the humidified CO was introduced to the anode, while air or O_2 was supplied to the cathode at a flow rate of 300 mL/min.

Electron transfer number and mass activity calculation

The electron transfer number was calculated using the Koutchy-Levich equation provided below at various rotation rates:

$$J_L = 0.2nFC_0\boldsymbol{\omega}^{1/2}(D_0)^{2/3}\upsilon^{-1/6} \quad (1)$$

Where J_L is the diffusion-limited current density, $\boldsymbol{\omega}$ is the electrode rotation rate (400,

625, 900, 1225, 1600, 2025 r), n is the electron transfer number, F Faraday constant (96485 C mol^{-1}), C_0 is the bulk concentration of CO (2), D_0 is the diffusion coefficient of CO and v is the kinetic viscosity of the electrolyte (3).

Calculate the mass activity using the following equation under different Rh loadings:

$$MA = \frac{i \cdot i_k}{|i_k - i| \cdot m}$$

i_k: Current in mA at 0.15V vs RHE;

i: limiting diffusion current in mA at 0.3V -0.5V;

m: mass of Rh, mg.

XAFS data analysis

Data reduction, data analysis, and EXAFS fitting is applied through Athena and Artemis software（4）. The energy calibration of the sample was conducted through a standard foil, which as a reference was simultaneously measured. For EXAFS modeling, The global amplitude EXAFS (CN, R, σ^2 and ΔE_0) were obtained by nonlinear fitting, with least-squares refinement, of the EXAFS equation to the Fourier-transformed data in R-space, using Artemis software, EXAFS of the foil is fitted and the obtained amplitude reduction factor S_0^2 value was set in the EXAFS analysis to determine the coordination numbers (CNs) in the scattering path in sample. The Debye-Waller factors and delta Rs are obtained based on the guessing parameters and constrained for paths. Wavelet transformation (WT) is also employed using the software package developed by Funke and Chukalina using Morlet wavelet with κ = 10, σ = 1 (5)(6).

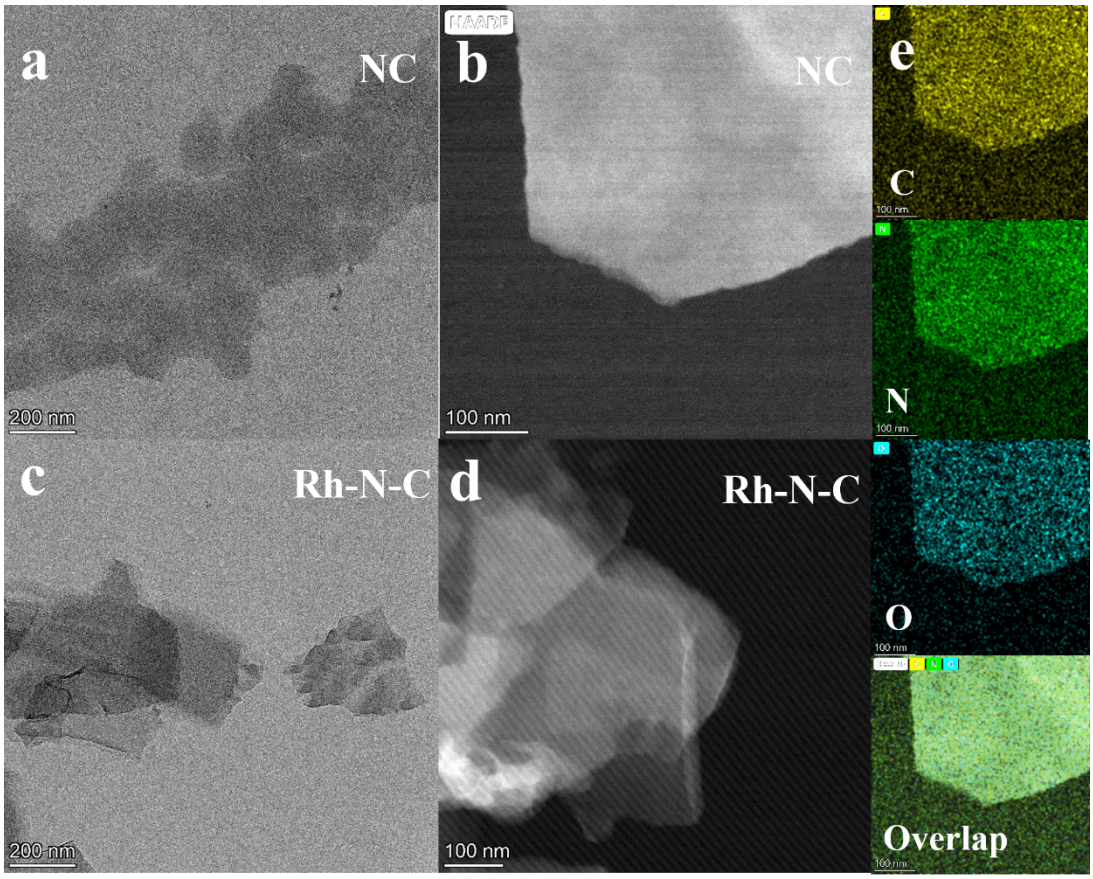

Figure S1. TEM images of NC (ab) and Rh-N-C (cd); (e) EDS mapping of NC. (All samples exist in the form of nanosheets, with elements such as C and N uniformly distributed on the NC.)

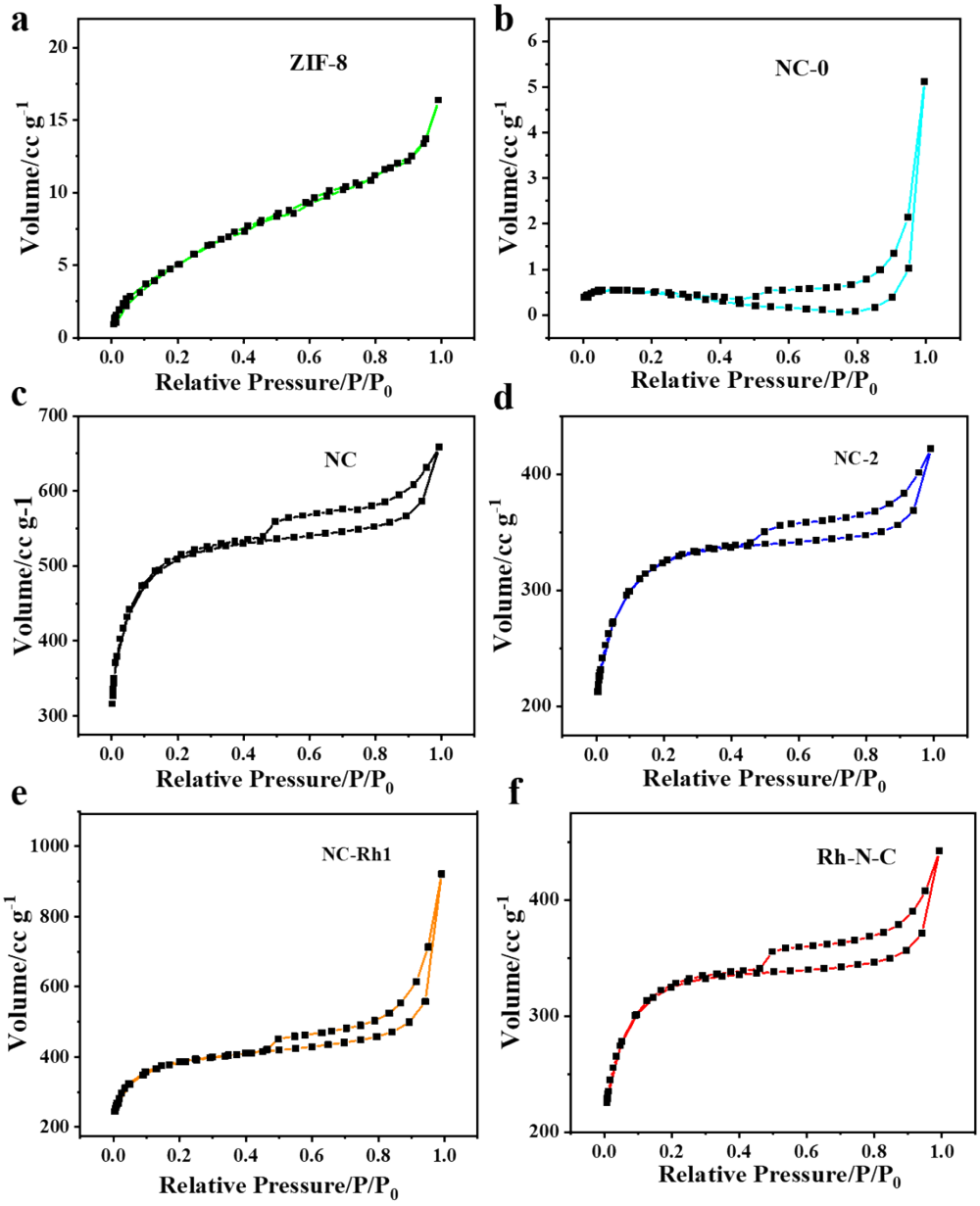

Figure S2. BET plots of Rh-N-C and the comparison samples. Specific surface area of a） ZIF-8, 21m^2/g; b) NC-0, 2.4 m^2/g; c) NC, 1887 m^2/g; d) NC-2, 1199 m^2/g; e) NC-Rh1, 1442 m^2/g; f) Rh-N-C, 1221 m^2/g.

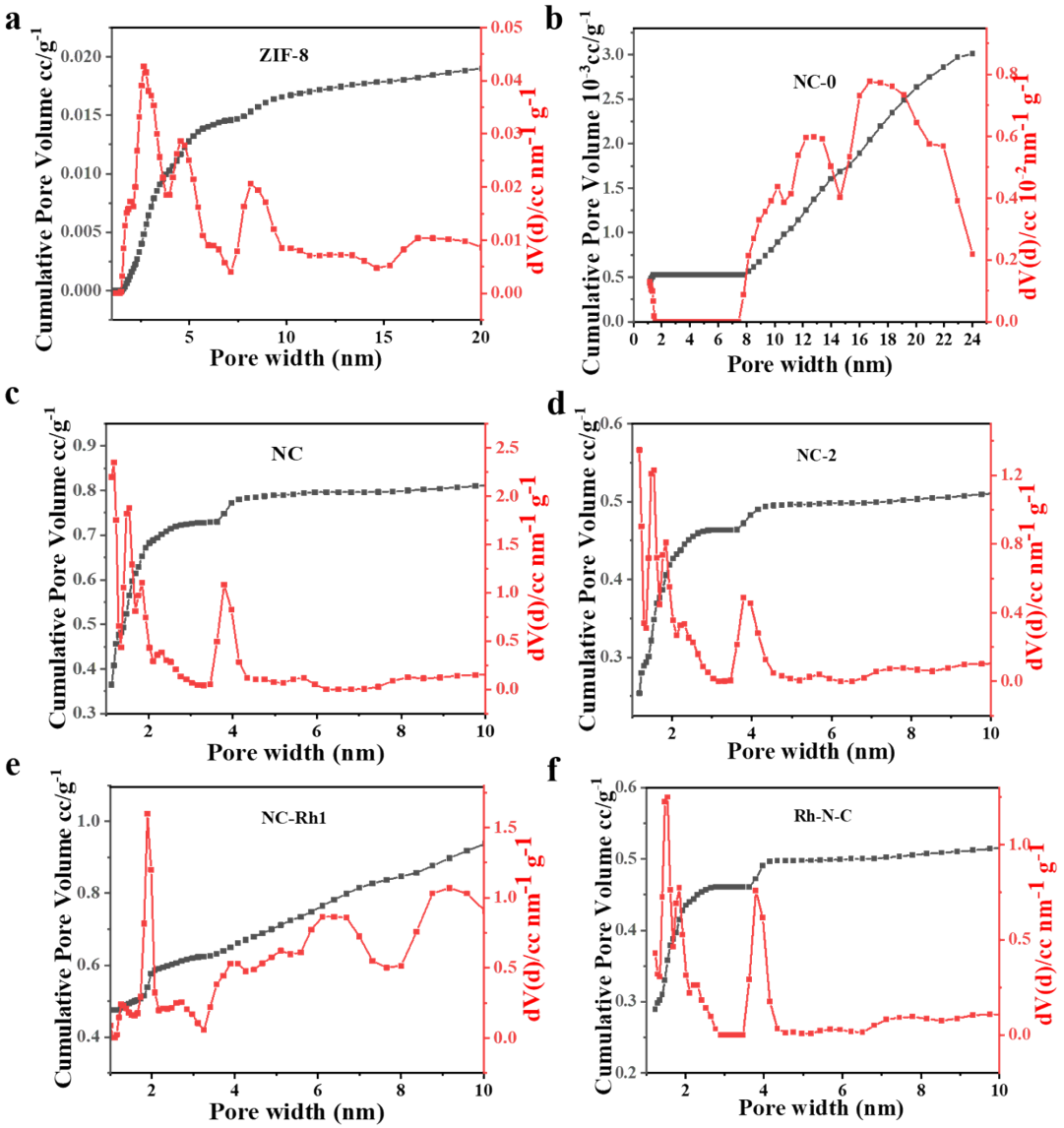

Figure S3. Pore size distribution of Rh-N-C and the comparison samples.

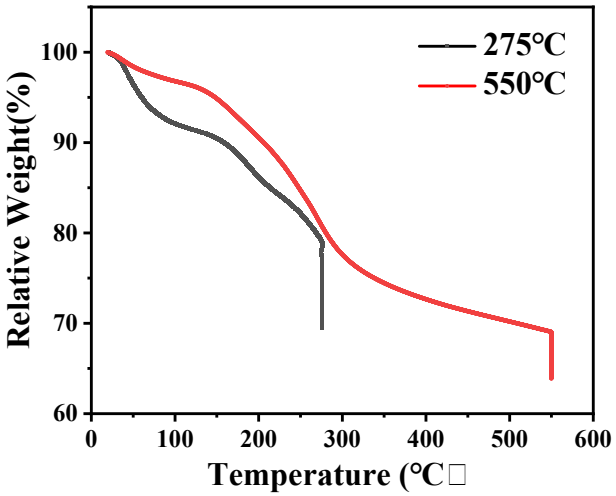

Figure S4. Thermogravimetric curve of Rh-N-C during the preparation process. The two curves represent the mass changes of the sample during two pyrolysis processes. The black curve corresponds to a heating rate of 5°C/min to 275°C, with the black vertical line indicating the mass change during a 5-hour holding period at 275°C. The red curve corresponds to a heating rate of 2°C/min to 550°C, with the red vertical line showing the mass change during a 5-hour holding period at 550°C. The results indicate that the sample continuously loses mass during the calcination process, which explains the enhanced Rh XRF signal after calcination in Figure 1d.

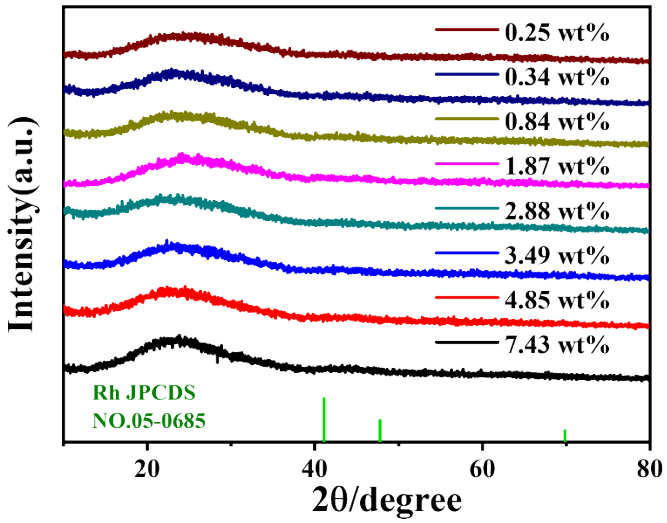

Figure S5. XRD patterns of Rh-N-C in different Rh loadings. (The XRD analysis indicates the successful synthesis of Rh-N-C catalysts with varying metal loadings, with no distinct diffraction peaks corresponding to nanoparticles observed.)

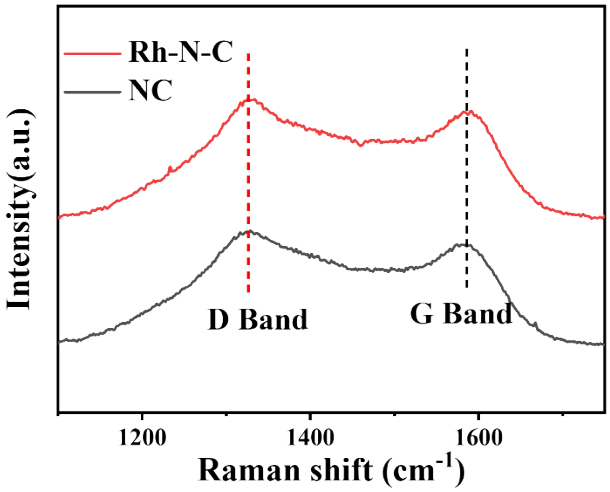

Figure S6. Raman spectra of Rh-N-C and NC. I_D/I_G: NC:1.07; Rh-N-C:1.08. (Raman spectra show that the graphitization degree of Rh-N-C is slightly lower than that of NC, which is attributed to the change of the graphitization structure of the carrier caused by the introduction of Rh element.)

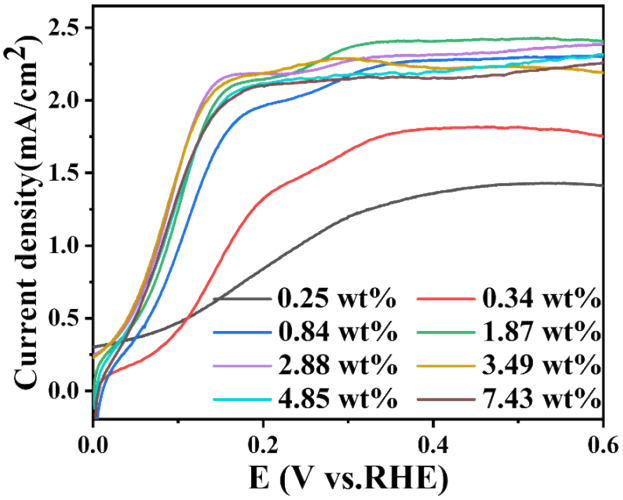

Figure S7. LSV curves of Rh-N-C in different loadings (LSV tests were carried out in CO-saturated 0.1M $HClO_4$ with a scan rate of 10 mV/s.).

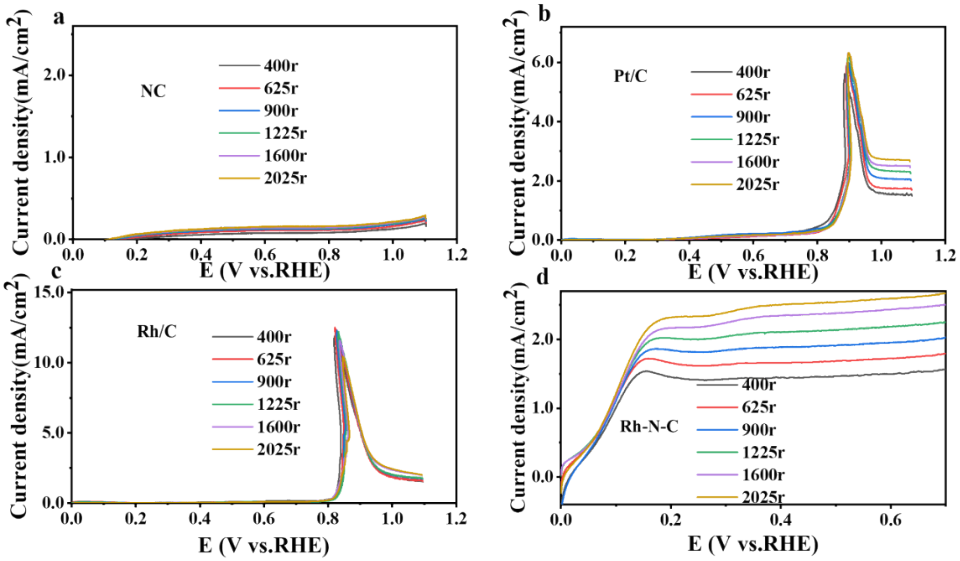

Figure S8. LSV curves of Rh-N-C（2.88w%）and comparison samples at different rotation speeds. a) NC; b) Pt/C; c) Rh/C; d) Rh-N-C. (LSV tests were carried out in CO-saturated 0.1M $HClO_4$ with a scan rate of 10 mV/s.).

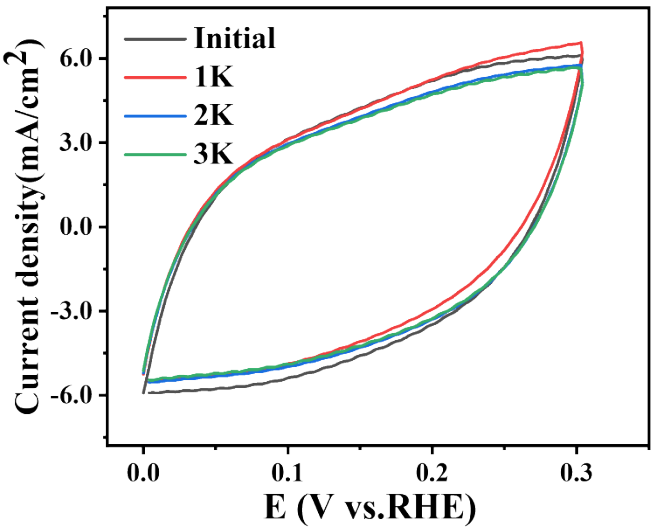

Figure S9. Stability test of Rh-N-C (Stability tests were performed in N_2-saturated 0.1M $HClO_4$, with cyclic voltammetry (CV) conducted for 3,000 cycles between 0–0.3 V vs. RHE at a scan rate of 100 mV/s.).

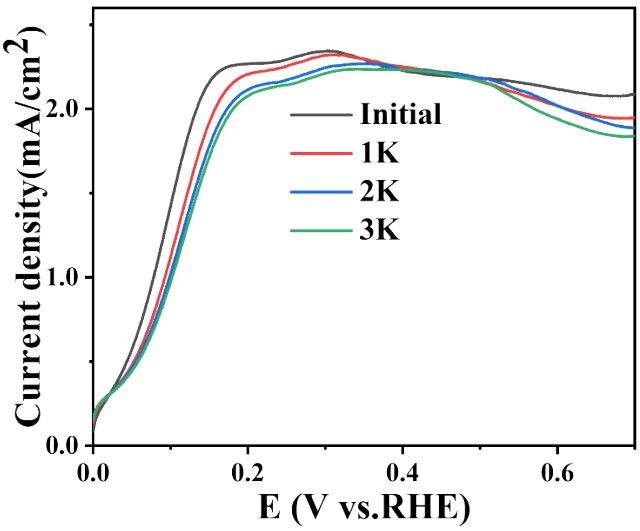

Figure S10. LSV curves obtained after every 1,000 cycles of CV scanning. (LSV tests were carried out in CO-saturated 0.1M $HClO_4$ with a scan rate of 10 mV/s.).

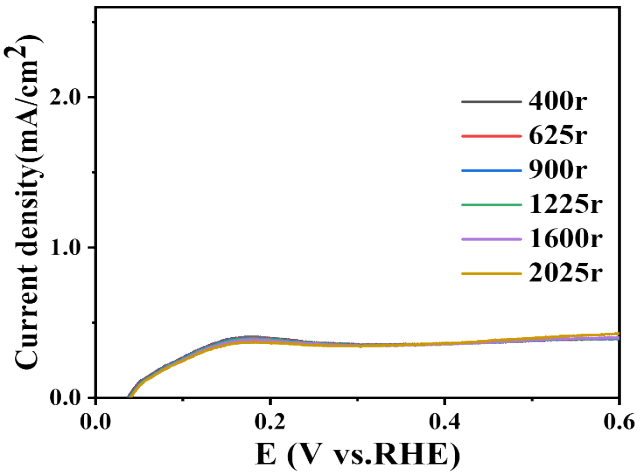

Figure S11. LSV curves of Rh-N-C (2.88wt%) under N_2-saturated conditions at different rotation speeds.

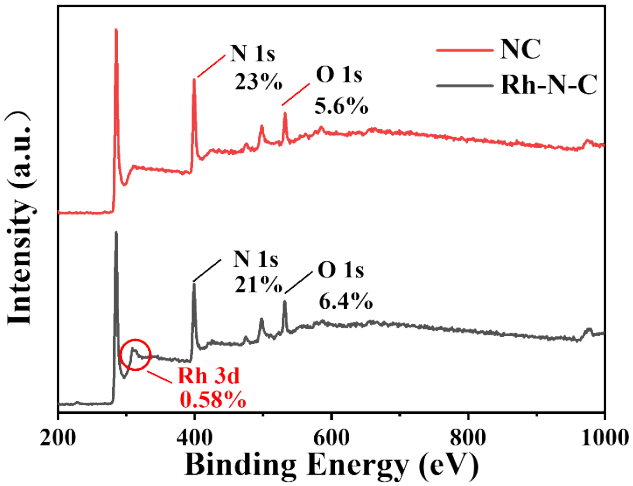

Figure S12. XPS full spectra of Rh-N-C and NC. (In the NC, besides C, N and O elements were detected; in Rh-N-C, besides C, Rh, N, and O elements were detected, with the N content reaching over 20%. The high nitrogen content provides a large number of active sites for the anchoring of Rh.)

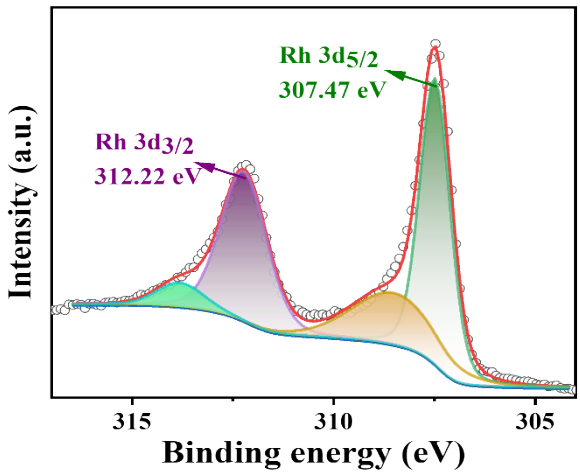

Figure S13. XPS peak fitting results of Rh/C. (The XPS spectrum of Rh nanoparticles shows two peaks at 312.22 eV and 307.47 eV, corresponding to the $3d_{3/2}$ and $3d_{5/2}$ peaks of metallic Rh, respectively.).

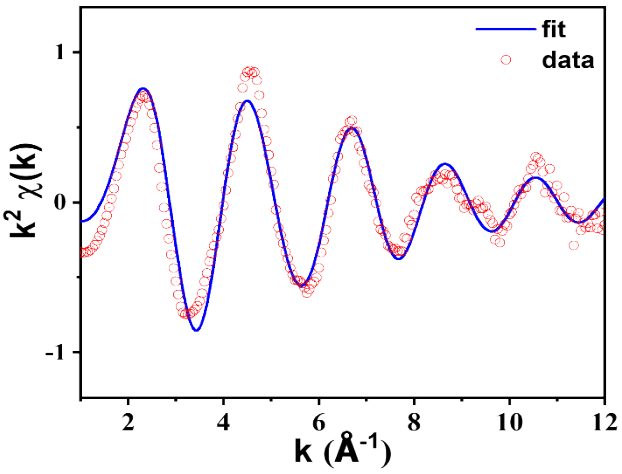

Figure S14. Comparison between the fitting results using RhN_4 as a model and experimental results.

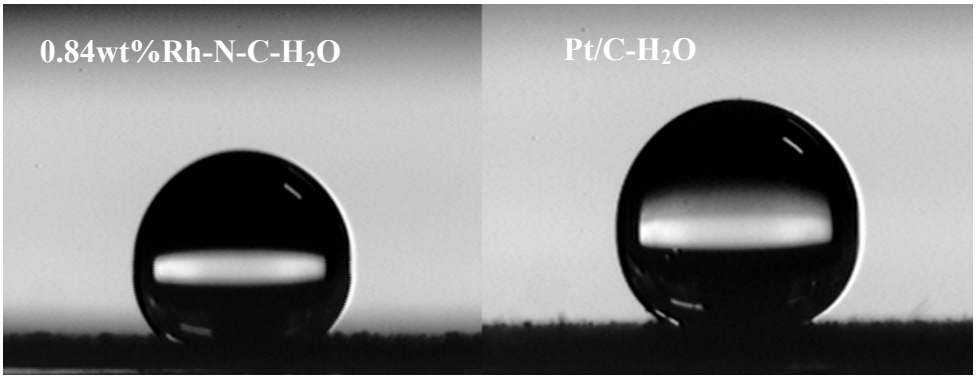

Figure S15. Contact angle of 0.84wt% Rh-N-C and Pt/C with water.

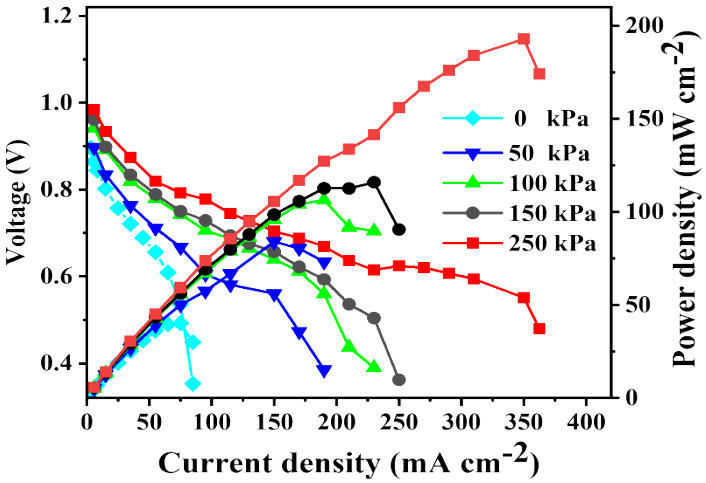

Figure S16. HT-PEMFC performance of Rh-N-C as the anode catalyst under different backpressures. (The cell temperature was 180°C, and the humidification temperature was 94°C (with the water vapor pressure at 0.8 atm). The flow rates of hydrogen and oxygen were both set to 300 mL/min.)

Table 1. Fitting parameters for Rh K-edge EXAFS for the sample.

[a] *CN*, coordination number; [b] *R*, the distance to the neighboring atom; [c] σ^2, the Mean Square Relative Displacement (MSRD); [d] ΔE_0, inner potential correction; *R* factor indicates the goodness of the fit. S_0^2 was fixed to 0.9823, according to the experimental EXAFS fit of the sample foil by fixing *CN* as the known crystallographic value. This value was fixed during EXAFS fitting, based on the known structure of Rh foil. Data range $3.0 \leq k \leq 10.0$ Å^{-1}, $1.0 \leq R \leq 2.0$ Å. The Debye-Waller factors and ΔRs are based on the *guessing* parameters and constrained for paths.

Sample	Shell	CN[a]	R(Å)[b]	σ^2(Å^2)[c]	ΔE_0(eV)[d]	S_0^2	R factor
Rh foil	Rh-Rh	12 (set)	2.68	0.005	-6.8±0.5	0.9823 (calculated)	0.017
sample	Rh-N	4.4±0.3	2.04	0.005	1.0±0.9	0.9823(set)	0.014

Reference:

(1) A. F. Starace, *Phys. Rev. B,* **1972**, *5* (5), 1773-1784.
(2) W. T. Napporn, J. M. Léger, C. Lamy, *J. Electroanal. Chem.* **1996**, *408* (1), 141-147.
(3) S. I. Yamazaki, T. Ioroi, Y. Yamada, K. Yasuda, T. Kobayashi, *Angew. Chem.,* **2006**, *45* (19), 3120-3122.
(4) B. Ravel, Newville,**2005**, *12* (4), 537-541.
(5) H. Funke, A. Scheinost, M. Chukalina, *Phys. Rev. B,* **2005**, *71* (9), 094110.
(6) H. Funke, M. Chukalina, A. C. Scheinost, *J. Synchrotron. Radiat,* **2007**, *14* (5), 426-432.